

## Sound radiation from an axisymmetric radiator in an infinite baffle

Hideo Suzuki\* and Jiri Tichy

*Applied Research Laboratory, The Pennsylvania State University,  
University Park, Pennsylvania 16802, U.S.A.*

(Received 25 August 1981)

A method that can be applied to the radiation problem of a convex or a concave radiator in an infinite baffle is described. This method utilizes the least square error method, and allows the radiator to take almost any kind of axisymmetric shape even though the accuracy of the result depends on the shape. The frequency responses of the on-axis sound pressure are calculated for three cases of the radiator shape, a convex dome, a concave dome, and a combination of a truncated concave cone and a convex dome at the center. The accuracy is confirmed by comparing the results obtained by the present method with those obtained by previous methods by the present authors. Three error indexes are suggested for an estimation of the accuracy of the results.

PACS number: 43. 20, 43. 88

### 1. INTRODUCTION

Recently, in several papers,<sup>1-5)</sup> the radiation characteristics of a concave radiator were discussed without the use of approximation methods such as the geometrical approximation or the plane-wave approximation. The results show that the diaphragm shape has significant effects on the radiation characteristics, even when it vibrates as a piston. Shindo *et al.* discussed the effect of the dust cap of a cone loudspeaker on its sound radiation using the finite element method.<sup>1)</sup> The finite element method was also used for a discussion of the sound radiation from a horn loudspeaker by Morita *et al.*<sup>2)</sup> In that study, the effect of different shapes of horns and phase plugs on the radiation characteristics were discussed. Ohie *et al.* discussed the radiation characteristics from a concave cylinder and a cone-shaped radiator.<sup>3,4)</sup> For the case of the cone-shaped radiator, the cavity was approximated by a combination of thin cylinders; the sound field was then expressed using cylindrical wave functions inside each cylinder. Suzuki and Tichy applied the least square error

method to the determination of the sound radiation from convex and concave domes in an infinite baffle.<sup>5)</sup> In that study, two different techniques were employed; the first for the radiation problem of convex domes, and the second for the radiation problem of concave domes. The radiation characteristics of convex and concave domes were compared with those of a flat piston.

This paper presents a method that can be applied to the radiation problem from an arbitrary shape of a radiator with axisymmetry. The results are compared with those obtained in Ref. 5), and the degree of accuracy is discussed.

### LIST OF SYMBOLS

- $A$ : radius of the radiator
- $E$ : error factor
- $H$ : height of the dome
- $M, N$ : maximum numbers of orders  $m$  and  $n$ , respectively
- $O$ : origin of the coordinate system
- $P_n(\ )$ ,  $P_n'(\ )$ : Legendre function of the first kind and order  $n$ , and its derivatives

\*Present address: CBS Technology Center, 227 High Ridge Road, Stamford, Connecticut 06905, U.S.A.

- $S^{(1)}$ : radiator surface
- $S^{(2)}$ : imaginary surface of the semi-sphere of radius  $A$
- $U_0$ : amplitude of the velocity of the radiator
- $U_\nu$ : velocity distribution normal to the radiator surface
- $a_n, b_{2m}$ : unknown coefficients
- $h_{2m}^{(2)}(\ )$ ,  $h_{2m}^{(2)'}(\ )$ : spherical Hankel function of the second kind and order  $2m$ , and its derivative
- $i, m, n$ : orders of functions
- $j$ : unit of complex number
- $j_n(\ )$ ,  $j_n'(\ )$ : spherical Bessel function of the first kind and order  $n$ , and its derivative
- $k$ : wavenumber
- $r$ : radius of the spherical coordinate system
- $u_\nu(\ )$ : particle velocity in the  $\nu$  direction
- $(x, y, z)$ : rectangular coordinate system
- $\Psi_n^{(1)}(\ )$ ,  $\Psi_n^{(2)}(\ )$ : functions defined on the surface  $S^{(1)}$  and  $S^{(2)}$ , respectively
- $\theta$ : cone angle of the spherical coordinate system
- $\theta_\nu$ : angle of the unit vector measured with respect to the  $z$ -axis
- $\nu$ : unit vector normal to the radiator surface
- $\eta$ :  $\cos \theta$
- $\psi_I, \psi_{II}$ : velocity potentials
- $\omega$ : angular frequency
- $*$ : complex conjugate

**2. GEOMETRY OF THE MODEL**

The cross section of the radiator model is shown in Fig. 1, where a rigid diaphragm with radius  $A$  is installed in the opening of an infinite baffle (corresponding to the  $xy$ -plane). The  $z$ -axis is the axis

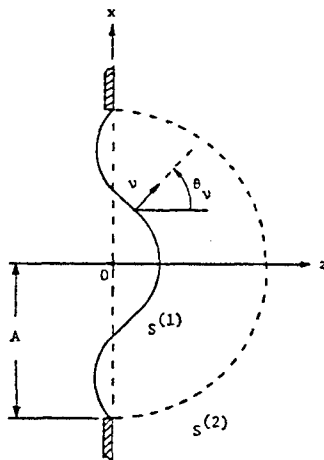


Fig. 1 Geometry of the model.

of revolution. In most cases, the spherical coordinate system  $(r, \theta, \phi)$  is used instead of the Cartesian coordinate system  $(x, y, z)$ . The radiator surface and the imaginary surface of a sphere of radius  $A$  and origin  $O$  are denoted by  $S^{(1)}$  and  $S^{(2)}$ , respectively. For the present case, the diaphragm is assumed to vibrate in the  $z$ -direction sinusoidally. Then, the velocity distribution normal to the diaphragm is given by  $U_\nu(r, \theta) = U_0 \cos \theta_\nu$ . The time dependent term  $e^{j\omega t}$  will be suppressed for simplicity.

**3. MATHEMATICAL DISCUSSION**

The velocity potential in the space surrounded by  $S^{(1)}$  and  $S^{(2)}$  is represented by

$$\psi_I(r, \theta) = \sum_{n=0}^{\infty} a_n j_n(kr) P_n(\cos \theta), \tag{1}$$

and the velocity potential in the semi-infinite space outside the sphere is represented by

$$\psi_{II}(r, \theta) = \sum_{m=0}^{\infty} b_{2m} h_{2m}^{(2)}(kr) P_{2m}(\cos \theta), \tag{2}$$

where only terms of even order are used in Eq. (2) since the normal velocity on the baffle surface is zero. The particle velocity on  $S^{(1)}$  in the direction of  $\nu$  is obtained by

$$\begin{aligned} u_\nu(r, \theta) &= - \left[ \frac{\partial \psi_I}{\partial r} \frac{\partial r}{\partial \nu} + \frac{\partial \psi_I}{\partial \theta} \frac{\partial \theta}{\partial \nu} \right] \\ &= \sum_{n=0}^{\infty} a_n \Psi_n^{(1)}(r, \theta), \end{aligned} \tag{3}$$

where

$$\begin{aligned} \Psi_n^{(1)}(r, \theta) &= - [k j_n'(kr) P_n(\cos \theta) \cos(\theta_\nu - \theta) \\ &\quad - j_n(kr) P_n'(\cos \theta) \sin \theta \sin(\theta_\nu - \theta) / r]. \end{aligned} \tag{4}$$

This must be equal to the prescribed velocity distribution. Thus, we have

$$\sum_{n=0}^{\infty} a_n \Psi_n^{(1)}(r, \theta) = U_0 \cos \theta_\nu. \tag{5}$$

On the surface  $S^{(2)}$ , the velocity potential and the particle velocity normal to the surface must be continuous, i.e.,

$$\psi_I(r, \theta)|_{r=A} = \psi_{II}(r, \theta)|_{r=A} \tag{6}$$

and

$$- \frac{\partial \psi_I(r, \theta)}{\partial r} \Big|_{r=A} = - \frac{\partial \psi_{II}(r, \theta)}{\partial r} \Big|_{r=A}. \tag{7}$$

From Eq. (7), we have

$$\begin{aligned} & \sum_{n=0}^{\infty} a_n j_n'(kA) P_n(\cos \theta) \\ &= \sum_{m=0}^{\infty} b_{2m} h_{2m}^{(2)'}(kA) P_{2m}(\cos \theta). \end{aligned} \quad (8)$$

Multiplying by  $P_{2i}(\cos \theta) \sin \theta$  and integrating from 0 to  $\pi/2$ , we obtain

$$\begin{aligned} & \sum_{n=0}^{\infty} a_n j_n'(kA) \int_0^1 P_n(\eta) P_{2i}(\eta) d\eta \\ &= \sum_{m=0}^{\infty} b_{2m} h_{2m}^{(2)'}(kA) \int_0^1 P_{2m}(\eta) P_{2i}(\eta) d\eta. \end{aligned} \quad (9)$$

Utilizing the property:

$$\begin{aligned} \int_0^1 P_{2m}(\eta) P_{2i}(\eta) d\eta &= 0 \quad \text{for } m \neq i, \\ &= \frac{1}{4i+1} \quad \text{for } m=i, \end{aligned} \quad (10)$$

$b_{2i}$  is expressed by

$$b_{2i} = \sum_{n=0}^{\infty} a_n j_n'(kA) \frac{4i+1}{h_{2i}^{(2)'}(kA)} \int_0^1 P_n(\eta) P_{2i}(\eta) d\eta. \quad (11)$$

Rewriting Eq. (6), we obtain

$$\begin{aligned} \sum_{n=0}^{\infty} a_n j_n(kA) P_n(\cos \theta) &= \sum_{n=0}^{\infty} a_n j_n'(kA) \\ &\cdot \left\{ \sum_{m=0}^{\infty} \frac{4m+1}{h_{2m}^{(2)'}(kA)} \left[ \int_0^1 P_n(\eta) P_{2m}(\eta) d\eta \right] \right. \\ &\cdot \left. h_{2m}^{(2)}(kA) P_{2m}(\cos \theta) \right\}. \end{aligned} \quad (12)$$

Then,

$$\sum_{n=0}^{\infty} a_n \Psi_n^{(2)}(A, \theta) = 0, \quad (13)$$

where

$$\begin{aligned} \Psi_n^{(2)}(A, \theta) &= j_n(kA) P_n(\cos \theta) - j_n'(kA) \\ &\cdot \left\{ \sum_{m=0}^{\infty} \frac{4m+1}{h_{2m}^{(2)'}(kA)} \left[ \int_0^1 P_n(\eta) P_{2m}(\eta) d\eta \right] \right. \\ &\cdot \left. h_{2m}^{(2)}(kA) P_{2m}(\cos \theta) \right\}. \end{aligned} \quad (14)$$

Now, if we truncate the order  $m$  and  $n$  by  $M$  and  $N$ , respectively, Eqs. (5) and (13) are not exactly satisfied, and we can define the error factor by

$$\begin{aligned} E &= \int_{S^{(1)}} \left| \sum_{n=0}^N a_n \Psi_n^{(1)}(r, \theta) - U_0 \cos \theta \right|^2 dS \\ &+ \alpha \int_{S^{(2)}} \left| \sum_{n=0}^N a_n \Psi_n^{(2)}(A, \theta) \right|^2 dS. \end{aligned} \quad (15)$$

This error factor contains two quantities which are different in dimensions. They are adjusted to have the same dimensions using the weighting factor  $\alpha$  of a positive value. The least square error method allows us to find the unknown coefficients  $a_n$  which minimize Eq. (15). This is done by differentiating Eq. (15) with respect to  $a_n$ ,  $n=0, 1, \dots, N$ , so that we obtain  $N+1$  simultaneous equations.

$$\begin{aligned} & \sum_{n=0}^N a_n \left[ \int_{S^{(1)}} \Psi_n^{(1)} \Psi_n^{(1)*} dS + \alpha \int_{S^{(2)}} \Psi_n^{(2)} \Psi_n^{(2)*} dS \right] \\ &= \int_{S^{(1)}} U_0 \cos \theta \Psi_n^{(1)*} dS, \end{aligned} \quad (16)$$

$$i=0, 1, 2, \dots, N.$$

If once the radiator shape and  $kA$  are given,  $\Psi_n^{(1)}$  and  $\Psi_n^{(2)}$  defined by Eqs. (4) and (14) are determined on  $S^{(1)}$  and  $S^{(2)}$ , respectively, and the integrals inside the bracket of the above equation are calculated. Then, the  $N+1$  simultaneous equations can be solved.

#### 4. RESULTS AND DISCUSSION

The discussion in the preceding section shows that this method does not have any requirement on the shape of the radiator except the one which is equal to or close to a convex or a concave semi-sphere. (The reason for this was discussed in Ref. 5.) As the examples of the numerical calculations, the frequency responses of the far-field on-axis sound pressure were calculated for the three types of radiator shapes Figs. 2(a), 2(b), and 2(c). The first two were chosen for comparison with the results of the previous work.<sup>5)</sup> The third was chosen as one of the arbitrary shapes of the radiator.

The numbers  $M$  and  $N$  used for the calculations were determined after several cut-and-tries. In all cases, they were 14 and 16 at  $kA=0.1$  and 26 and

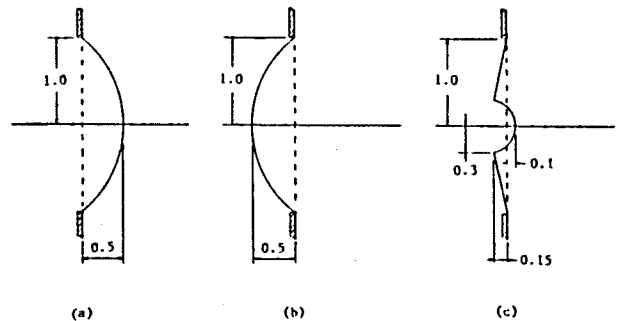
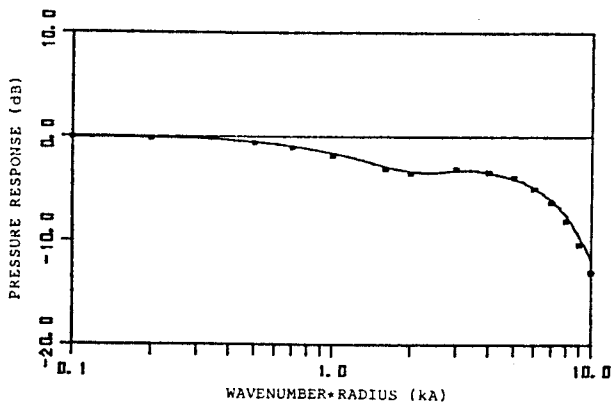
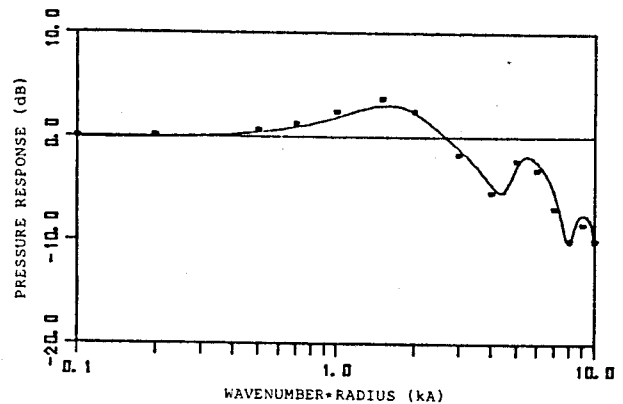


Fig. 2 Three types of radiator used for the calculation of far-field on-axis pressure.



**Fig. 3** Frequency response of the far-field on-axis pressure of a convex dome with  $H/A=0.5$  (type (a)). The solid line and the squares were calculated by the present and the previous methods, respectively.



**Fig. 4** Frequency response of the far-field on-axis pressure of a concave dome with  $H/A=0.5$  (type (b)). The solid line and the squares were calculated by the present and previous methods, respectively.

36 at  $kA=10.0$ , respectively. They increased almost linearly with respect to  $\log(kA)$  between these frequencies. The weighting factor  $\alpha$  in Eq. (15) was chosen equal to  $\omega$ , after the careful investigation of the effect of  $\alpha$  on the accuracy. The two sets of functions  $\Psi_n^{(1)}$  and  $\Psi_n^{(2)}$  in Eq. (15) are frequency dependent, and in the present problem it was found that  $\alpha$ , when let equal to  $\omega$ , gave the best accuracy among the cases tested.

The far-field on-axis sound pressure of the convex dome with a height-to-radius ratio ( $H/A$ ) equal to 0.5, which was normalized to the response of a flat piston with same volume velocity (0 dB line) was obtained by the present method and also by the previous method.<sup>5)</sup> Figure 3 shows that the two curves are in good agreement with each other except in the high-frequency region. The far-field on-axis sound pressures of the concave dome obtained by these two methods are compared in Fig. 4. The discrepancies between the responses are larger than for those of the convex dome. The reason for this may be the lack of accuracy in the numerical calculation of the Rayleigh integral, which had been used in the previous method.<sup>5)</sup> The results which were obtained by both methods, however, are reasonably accurate descriptions of the radiation characteristics of convex and concave domes.

The radiator shown in Fig. 2(c) has a compound shape comprising a truncated cone and a convex dome. The main difference between this shape and the previous two types is that it has surfaces both

behind and in front of the baffle surface. The frequency response of the normalized far-field on-axis sound pressure of this radiator is shown in Fig. 5. This result seems reasonable, because a shallow radiator should have a response close to that of a flat piston which is given by the 0 dB line.

The errors of the methods stated above may be estimated by checking the degree of matching of the velocity potentials and particle velocities. The following three errors were calculated:

$$\text{ERROR 1} = \int_{S^{(1)}} \left| \left[ \sum_{n=0}^N a_n \Psi_n^{(1)}(r, \theta) \right] - U_v(r, \theta) \right|^2 dS + \int_{S^{(1)}} \left| \sum_{n=0}^N a_n \Psi_n^{(1)}(r, \theta) \right|^2 dS, \quad (17)$$

$$\text{ERROR 2} = \int_{S^{(2)}} \left| \left[ \sum_{n=0}^N a_n j_n(kA) P_n(\cos \theta) \right] - \left[ \sum_{m=0}^M b_{2m} h_{2m}^{(2)}(kA) P_{2m}(\cos \theta) \right] \right|^2 dS + \int_{S^{(2)}} \left| \sum_{n=0}^N a_n j_n(kA) P_n(\cos \theta) \right|^2 dS, \quad (18)$$

and

$$\text{ERROR 3} = \int_{S^{(2)}} \left| \left[ \sum_{n=0}^N a_n k j_n'(kA) P_n(\cos \theta) \right] - \left[ \sum_{m=0}^M b_{2m} k h_{2m}^{(2)'}(kA) P_{2m}(\cos \theta) \right] \right|^2 dS + \int_{S^{(2)}} \left| \sum_{n=0}^N a_n k j_n'(kA) P_n(\cos \theta) \right|^2 dS. \quad (19)$$

ERROR 1 and 3 give the degree of matching of the velocities on the surfaces  $S^{(1)}$  and  $S^{(2)}$ , respectively. ERROR 2 calculates the error of the matching of the velocity potentials on  $S^{(2)}$ . The results of ERROR 1, 2, and 3 for the three different diaphragms are plotted in Figs. 6~8.

ERROR 1, 2, and 3 of the convex and concave domes are mostly less than 0.01. The convex and concave domes show different frequency dependent errors and, generally speaking, the convex dome has a better accuracy. Since the sound fields around the convex and concave domes are different from each other,<sup>5)</sup> it may be necessary to use different values of  $M$  and  $N$  in order to have the same order of accuracy.

ERROR 1, 2, and 3 for the compound radiator type (c) increase gradually above  $kA=2.0$ . An error peak is seen at  $kA=4$ , and beyond this fre-

quency ERROR 1 is greater than 0.01. This type of error peak is mostly induced when one (or both) of  $M$  and  $N$  are given a too large value (or values). The spherical Bessel and Neumann functions (and their derivatives) become very small and very large, respectively, for a given value of argument as their order increases. This nature of these functions is the main cause of the errors in the numerical calculation of the present method. An error peak such as observed in Fig. 6 or 8 occurs at an unpredicted frequency even if the same set of  $M$  and  $N$  gives reasonable accuracy in the range around that specific frequency. For this reason, the accuracy of the results should be checked for each frequency of the calculation. ERROR 1, 2, and 3 defined by Eqs. (17)~(19) seem to be suitable for this purpose. The sound pressure

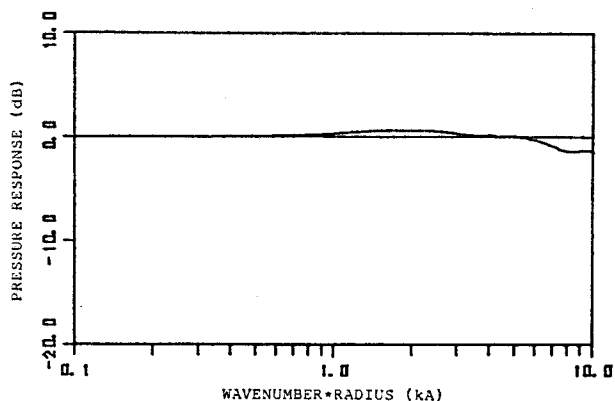


Fig. 5 Frequency response of the far-field on-axis pressure of a compound radiator (type (c)).

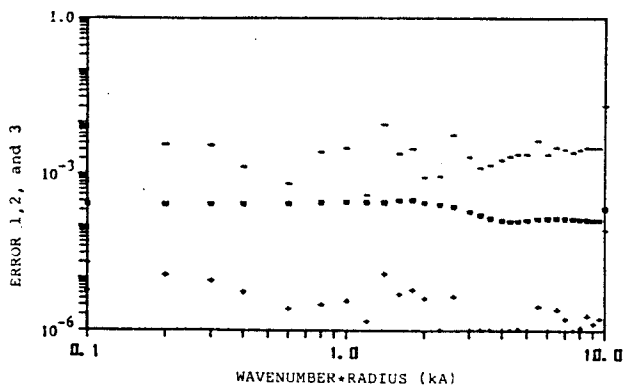


Fig. 6 Frequency dependence of errors in the calculation of the pressure of the convex dome (type (a)). The square, plus, and minus signs are for ERROR 1, 2, and 3, respectively.

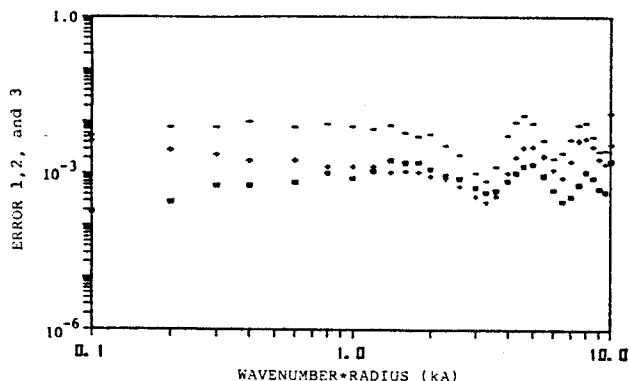


Fig. 7 Frequency dependence of errors in the calculation of the pressure of the concave dome (type (b)). The square, plus, and minus signs are for ERROR 1, 2, and 3, respectively.

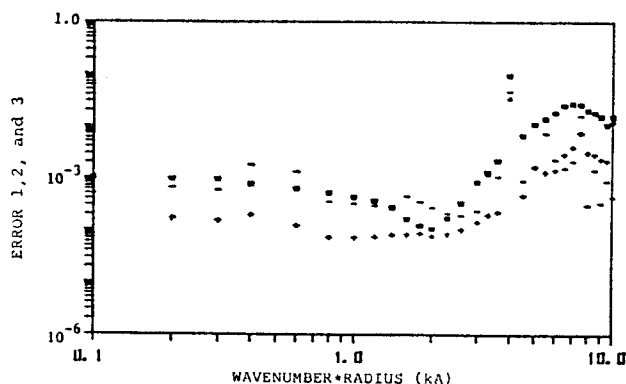


Fig. 8 Frequency dependence of errors in the calculation of the pressure of the compound radiator (type (c)). The square, plus, and minus signs are for ERROR 1, 2, and 3, respectively.

at  $kA=4.0$  in Fig. 5 does not differ much from those at the adjacent frequencies, even though the corresponding errors at this frequency are much larger than the neighbors (ERROR 1 in Fig. 8 is almost 0.1 at  $kA=4.0$ ). (It was confirmed that a usage of smaller values of  $M$  and  $N$  at  $kA=4.0$  gives better accuracy.)

From the above discussion it can be concluded that if ERROR 1, 2, and 3, defined by Eqs. (17)~(19), respectively, are not larger than 0.01, the result obtained has sufficient accuracy for the determination of the radiation characteristics at the frequency of interest.

### 5. CONCLUSIONS

A method that can be applied to the radiation problem from a radiator of an arbitrary shape (axisymmetric) has been presented. The on-axis sound pressures of the convex and concave domes have been compared with those obtained in the previous paper,<sup>3)</sup> and it is concluded that the accuracy of the present method is sufficient for the determination of the radiation characteristics of the convex and concave radiators. This method was also applied to the radiation problem from a very shallow radiator consisting of convex and concave surfaces. It has been shown that this method gives reasonable result which is close to the on-axis sound pressure of the flat piston over the range  $kA=0.1\sim 10.0$ .

The accuracy of the present method was estimated by checking the degree of continuity of the particle velocities and velocity potential of the solution. If ERROR 1, 2, and 3 defined by Eqs. (17)~(19), respectively, are not larger than 0.01, the result may have sufficient accuracy for the discussion of the radiation characteristics.

The present method can also be applied to the radiation problem from a thin shell or a plate vibrating with a prescribed velocity distribution, by introducing both the even and odd terms in Eq. (2) and taking the integration in Eq. (9) over the range  $-1$  to  $1$ . In this paper, only axisymmetric cases were considered. It may be straightforward to apply this method to a three-dimensional problem.

### ACKNOWLEDGEMENTS

The authors wish to thank Earl R. Geddes and Arthur W. Horback, of the Graduate Program in Acoustics of the Pennsylvania State University, for their assistance in the English revision. This study was supported by Applied Research Laboratory, The Pennsylvania State University.

### REFERENCES

- 1) T. Shindo, N. Kyono, O. Yashima, T. Yamabuchi, and Y. Kagawa, "The role of the dust cap in the cone-type loudspeaker," Preprint for the 63rd Convention of Audio Eng. Soc., Los Angeles (1979).
- 2) S. Morita, N. Kyono, S. Sakai, T. Yamabuchi, and Y. Kagawa, "Acoustic radiation of a horn loudspeaker by the finite element method—A consideration of the acoustic characteristic of horns," *J. Audio Eng. Soc.* 28, 482-489 (1980).
- 3) S. Ohie, H. Suzuki, and T. Shindo, "Sound radiation from a concave radiator in an infinite baffle," *J. Acoust. Soc. Jpn.* 34, 429~435 (1978) (in Japanese).
- 4) S. Ohie, R. Takeuchi, and T. Shindo, "Sound radiation from a concave radiator in an infinite baffle," *Acustica* 46, 268-275 (1980).
- 5) H. Suzuki and J. Tichy, "Sound radiation from convex and concave domes in an infinite baffle," *J. Acoust. Soc. Am.* 69, 41-49 (1981).